



SEISMIC SCENARIO SPECIFIC GROUND MOTION SIMULATIONS CONSISTENT WITH GROUND MOTION PREDICTION EQUATION

V.L. Nithin⁽¹⁾, S. Das⁽²⁾, H.B. Kaushik⁽³⁾

⁽¹⁾Graduate Student, Department of Civil Engineering, IIT Guwahati, India, nithin.l@iitg.ernet.in

⁽²⁾Assistant Professor, Department of Civil Engineering, IIT Guwahati, India, sandip.das@itg.ernet.in

⁽³⁾Associate Professor, Department of Civil Engineering, IIT Guwahati, India, hemanthk@iitg.ernet.in

Abstract

In seismic hazard analysis ground motion prediction equations (GMPEs) play a pivotal role. For that reason, there are many such GMPEs available for different regions. However, GMPEs provide elastic spectral quantities or other ground motion intensity measures. They do not give any temporal waveform information of ground motions, which is needed for carrying out nonlinear time-history analyses in order to obtain statistical estimates for the structural response. Nevertheless, hazard posed at a given site is usually characterized by elastic spectral quantities from a suitable GMPE. However, no methods are presently available to get ensemble of simulated motions strictly compatible to any target GMPE so that the detailed statistical analysis directly at the response level can be carried out while still being consistent to the hazard posed at that site. A new method is proposed here to characterize the time-frequency characteristics of ground motions via instantaneous energy arrival of wavelet coefficients. Further, the energy arrival patterns are extracted from ground motions corresponding to different magnitudes, source to site distances and local site conditions, and a scaling model for energy arrival pattern based on seismological parameters is developed. Thus, energy arrival patterns for a given seismic scenario are estimated considering their inherent uncertainty and using a proposed reconstruction procedure an ensemble of ground motions for that scenario is simulated. It is found that the median of the linear spectra obtained from such a simulated ensemble is comparable with that obtained independently from a GMPE developed for the same ground motion database. A new method is also proposed by which the energy arrival curves are modified such that the median and standard deviation of linear spectra obtained from the simulated ensemble will closely match those from the target GMPE. In the present study a scaling model for pseudo spectral velocity (PSV) spectrum for 5% damping is considered as the target GMPE. The GMPE-compatible ensemble is found to be in good agreement with the PSV scaling model in terms of median and standard deviation of response spectra. It is further found that the same GMPE-compatible ensemble, developed for 5% damping PSV spectrum, remains naturally consistent with PSV scaling models developed for a wide range of damping ratio provided, all the PSV scaling models are developed using the same ground motion database.

Keywords: Wavelet Coefficients, Energy Arrival, Amplitude Modulation, Scenario-Specific, GMPE-Compatible

1. Introduction

Ground motion prediction equations (GMPE) give the seismic hazard at a site for specific hazard parameters. The hazard parameters are usually spectral quantities like spectral acceleration (SA), pseudo spectral velocity (PSV) [1, 2], or sometimes other intensity measures like peak ground acceleration (PGA), strong motion duration (SMD) [3]. Detailed nonlinear time-history analysis is often required in the earthquake resistant design of structures to check the design adequacy [4, 5]. If the adequacy is intended to be checked with a level of confidence, then a statistical estimate is necessary for the nonlinear response, which is not provided by the GMPEs. Nevertheless, ground motions that are consistent to the site-specific GMPE should only be considered for the nonlinear analysis so that the check for structural adequacy corresponds to the hazard posed at the site.

Recently Yamamoto and Baker [6] proposed a method for ground motion simulation using wavelet packet transform where the simulated motions for a chosen seismic scenario conform to a GMPE, when the latter is developed using the same dataset that has been considered for the simulation. Vetter et al [7] recently proposed a tuning method that makes stochastically simulated motions consistent with any target GMPE in terms of the median level prediction. Other studies are also available where ground motions are selected such that they closely emulate the statistics of scenario specific response spectra as predicted by a target GMPE [8, 9, 10]. Stochastic simulation based on frequency dependent amplitude modulation, as an approximation for a more general Priestly process [11] can be regarded as simple and yet quite effective. Conte and Peng [12] proposed a parametric model for frequency dependent unimodal amplitude modulation for generating simulated samples for the process of a recorded motion based on Priestley process assumption. Das and Gupta [13] proposed a wavelet-based methodology to extract frequency dependent unimodal amplitude modulations and to simulate a scenario-specific motion under a deterministic framework for the recording process. Iyama and Kuwamura [14] proposed a wavelet-based methodology to characterize the temporal features of earthquake ground motions via frequency dependent normalized S-shaped energy arrival curve, Fourier spectrum and frequency-wise predominant time.

Till date, there is no technique available that can extract the hidden frequency dependent modulation of a recorded motion non-parametrically via a frequency dependent ground motion intensity measure. This intensity measure can be estimated using a scaling relationship that can be used to simulate scenario specific ensemble of ground motions under a probabilistic framework. The estimated modulations can be then tuned to generate GMPE-compatible ensemble, which will emulate the statistics of a target GMPE.

In the present study, an attempt is made to simulate scenario specific motions with realistically varied time-frequency characteristics. Any recorded ground motion is first transformed into the wavelet domain and the temporal features of the ground motion are characterized by the frequency dependent (level-wise) amplitude modulation, derived from the frequency dependent instantaneous energy arrival of wavelet coefficients. Then a method is developed to generate samples for the recording process using the extracted modulations along with random samples of narrowband-limited white-noise signal corresponding to different frequency bands. Further, an attenuation relationship is proposed for the level-wise energy arrival curve via seismic scenario defining parameters. The scenario dependent estimated energy arrival along with the variations is directly used for the generation of scenario-specific different ground motion samples. Finally, a new algorithm is proposed to modify the estimated level-wise energy arrival such that the scenario-specific simulated ensemble becomes compatible with a target PSV scaling model, both in terms of median estimates and standard deviations. The results of the current study will provide GMPE-compatible ground motions using which any nonlinear response quantity can be statistically analyzed.

2. Stochastic characterization of ground motion

Wavelet analysis is very useful for characterization of fully nonstationary ground acceleration process because wavelet coefficients capture adequate information about both time and frequency description of a motion. In the present study, the modified Littlewood-Paley (L-P) wavelet basis as proposed by Basu and Gupta [15] has been used because these level-wise wavelet basis functions are strictly narrowband-limited in frequency domain. A brief review of the wavelet transform with essential details is provided next for the sake of completeness.

2.1 Mathematical Background on Wavelet Transform

Any finite energy signal, $f(t)$, can be transformed into wavelet domain and reconstructed back from there by using the wavelet transformation and the inverse wavelet transformation, respectively. The continuous wavelet transformation of $f(t)$ is defined with respect to a real wavelet basis, $\psi_{a,b}(t)$, as

$$W_{\psi}f(a, b) = \langle f, \psi_{a,b} \rangle = \int_{-\infty}^{\infty} f(t)\psi_{a,b}(t)dt \quad (1)$$

where,

$$\psi_{a,b}(t) = \frac{1}{a^{1/2}}\psi\left(\frac{t-b}{a}\right) \quad (2)$$

and $\psi(t)$ is called the mother wavelet.

Here, $a > 0$, the scale parameter, controls the frequency content of the dilated wavelet basis, and $b \in \mathfrak{R}$, the shift parameter, localizes the basis at $t = b$. The function $f(t)$ can be reconstructed back from the wavelet coefficients, $W_{\psi}f(a, b)$, as

$$f(t) = \frac{1}{2\pi C_{\psi}} \int_{-\infty}^{\infty} \int_{-\infty}^{\infty} \frac{1}{a^2} W_{\psi}f(a, b) \psi_{a,b}(t) da db \quad (3)$$

with

$$C_{\psi} = \int_{-\infty}^{\infty} \frac{|\hat{\psi}(\omega)|^2}{\omega} d\omega < \infty \quad (4)$$

In Eq. (4), $\hat{\psi}(\omega)$ is the Fourier transform of the basis function, $\psi(t)$, defined as

$$\hat{\psi}(\omega) = \frac{1}{\sqrt{2\pi}} \int_{-\infty}^{\infty} \psi(t) e^{-i\omega t} dt \quad (5)$$

In the present study, the modified L-P wavelet basis is used, for which the mother wavelet is defined as

$$\psi(t) = \frac{1}{\pi\sqrt{\sigma-1}} \frac{\sin(\sigma\pi t) - \sin(\pi t)}{t} \quad (6)$$

with σ taken as $2^{1/4}$ [15]. On discretizing and taking $a_j = \sigma^j$, where j is the index of (dilation) level, the wavelet coefficient corresponding to j th level is expressed by

$$W_{\psi}f(a_j, b) = \langle f, \psi_{a_j,b} \rangle = \int_{-\infty}^{\infty} f(t)\psi_{a_j,b}(t)dt \quad (7)$$

Further, $W_{\psi}f(a_j, b)$ has energy in the period band $(2a_j/\sigma, 2a_j)$ s and it can be considered as a narrowband signal in b . Typically, $W_{\psi}f(a_j, b)$ looks like an amplitude modulated signal of pseudo period $T_j (= 0.5(2a_j/\sigma + 2a_j))$. A total number of 32 levels are considered with $j = -21$ to 10, so that $W_{\psi}f(a, b) (= \sum_{j=-21}^{10} W_{\psi}f(a_j, b))$ spans over the period band (0.044-11.32)s which is sufficient for any earthquake signal. Further, for practical purpose of reconstruction, it is sufficient to consider a range for b which will start 12 s before the beginning of a signal and end 12 s beyond the endpoint of the signal. It may be noted that, any level-specific reconstructed motion, $f_j(t)$ (obtained by inverse transform of $W_{\psi}f(a_j, b)$ only without summation over j), from any Gaussian white-noise signal becomes a band-limited Gaussian white-noise within the narrow period range $(2a_j/\sigma, 2a_j)$ s.

2.2 Stochastic Simulation of Ground Motions

A random nonstationary process, $F(t)$, like earthquake ground motion process can be modelled as Priestley process [11]:

$$F(t) = \int_{-\infty}^{\infty} A(t, \omega) e^{i\omega t} \overline{dZ}(\omega) \quad (8)$$

where, $A(t, \omega)$ is a frequency dependent deterministic slow varying amplitude modulation and $\overline{dZ}(\omega)$ is a stationary orthogonal incremental process. Hence, it can be inferred that a nonstationary signal, $f(t)$, for the $F(t)$ process can be simulated using several narrowband-limited white-noise signals and different deterministic slow varying amplitude modulations, specific for the corresponding frequency bands as [12]

$$f(t) = \sum_j A_j(t) z_j(t) \quad (9)$$

where, $A_j(t)$ is the deterministic amplitude modulation specific to the j th frequency band and $z_j(t)$ is the corresponding band-limited white-noise signal. It should be mentioned that all piece-wise frequency bands are disjoint and exhaustive over the entire frequency range of $f(t)$. Since, the Priestley process assumption equally holds good in wavelet domain [16], Eq. (9) is also applicable for the wavelet coefficients. Hence, different samples for the observed $W_\psi f(a_j, b)$ process can be generated as

$$\widehat{W}_\psi f(a_j, b) = V_j(b) z_j(b) ; \forall j \quad (10)$$

where, $V_j(b)$ is the hidden deterministic amplitude modulation of the $W_\psi f(a_j, b)$ process and $z_j(b)$ is a random sample of a narrowband-limited Gaussian white-noise with period range $(2a_j/\sigma, 2a_j)$ s. $V_j(b)$ can be extracted from the smoothed form of energy arrival curve, $\overline{E}_j(b)$, of wavelet coefficients and its normalized shape is found to be proportional to $\sqrt{d\overline{E}_j(b)/db}$ for various observed wavelet coefficients. $V_j(b)$ is therefore proposed as

$$V_j(b) = \gamma_j \left[\frac{d\overline{E}_j(b)}{db} \right]^{\frac{1}{2}} \quad (11)$$

where γ_j is the unknown level-dependent proportionality constant. The normalized shape of $V_j(b)$ is used for the simulation of wavelet coefficient and the total energy of the simulated wavelet coefficient (see Eq. 10) is matched with that of the observed one. Hence, there is no need to know γ_j explicitly once $\widehat{W}_\psi f(a_j, b)$ (from Eq.10) is suitably scaled. For $j = 7$ to 10, Eq. (11) does not produce good results because the pseudo periods of the wavelet coefficients in those bands are long enough not to capture their modulation within the duration of recorded motions [13]. $V_j(b)$ s for the last four levels are assumed to be constant along b , which is not a serious limitation as the energy associated with each of these levels is usually very small.

In the present study, $z_j(b)$ that is considered as a narrowband-limited Gaussian white-noise signal usually exhibits beat-like phenomenon by forming many prominent slow varying loops of varying amplitude (like what is exhibited by wavelet coefficients of a recorded motion). Hence, proper localization of $z_j(b)$ needs to be done, before applying in Eq. (10), else, most of the samples will not impart the observed amplitude modulation. During localization, a tolerance is allowed on either side of the largest peak of $V_j(b)$ where a peak of a slow-varying loop of $z_j(b)$, lying above 2 x root-mean-square (r.m.s.) threshold, can randomly lie. The tolerance is made equal to T_j arbitrarily to add some desired variability among the random samples. The threshold of 2 x r.m.s. is chosen, arbitrarily, to avoid relatively small amplitude loops getting aligned with the peak of the modulation, otherwise, it will dilute the amplitude modulation in most of the samples. Fig.1(a) shows a schematic diagram explaining the method of generation of sample wavelet coefficients. Fig.1(b) shows the wavelet coefficient of a recorded motion (recorded during the main event at station C041 along east-west direction) for $j = -7$, a simulated

sample of wavelet coefficient using the proposed localization, and a simulated sample of wavelet coefficient without any localization constraint for the same level. Extracted modulation (properly scaled) of the wavelet coefficient of the recorded motion is shown in the figure. It is clear from the figure that the simulated sample using the proposed localization preserves the hidden modulation whereas the one without localization restriction fails to capture the amplitude modulation of the recorded wavelet coefficients. By taking the wavelet inverse transform of $\widehat{W}_\psi f(a, b) (= \sum_{j=-21}^{10} \widehat{W}_\psi f(a_j, b))$ using Eq. (3), a random sample for the recorded motion process is generated.

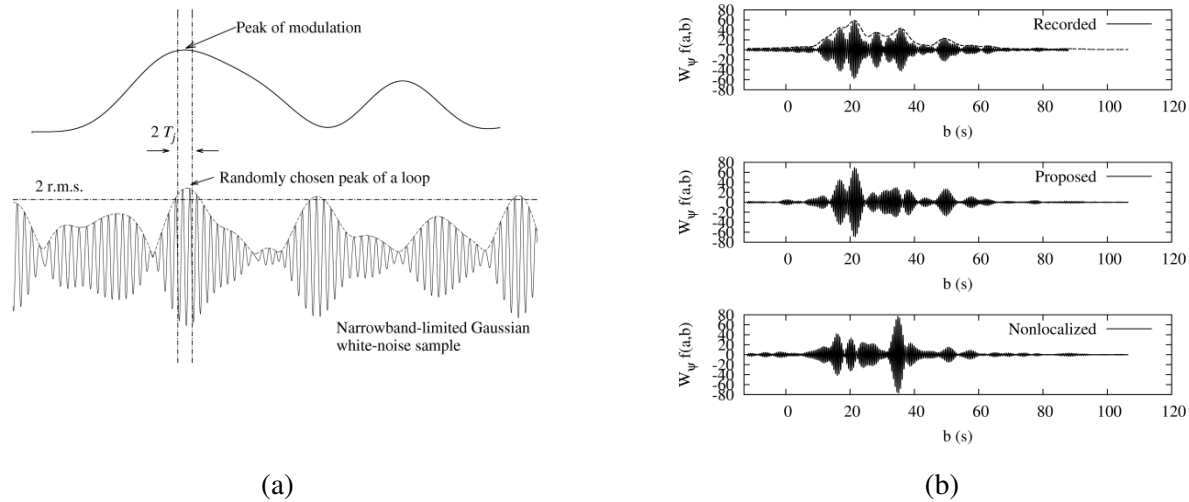


Fig. 1 – (a) Schematic Diagram for the proposed Localization Technique and (b) Recorded Wavelet Coefficient (with modulation shown in dotted line) at Station C041 along with Simulated Wavelet Coefficients using different Schemes, all for $j = -7$

2.3 Validation of Sample Generation Specific to a Recording Process

For validation, a motion recorded during the 1999 Chi-Chi main event at station C041 along east-west direction is chosen and its normalized amplitude modulations are extracted and 500 samples of ground motions are simulated. PSA spectra for 5% damping ratio of the 500 ground motion samples are computed. Fig.2 shows 5, 50 and 95 percentiles and minimum and maximum spectra and the PSA spectrum of the recorded motion. It can be observed that the minimum and maximum levels of response are able to capture the recorded trend quite satisfactorily. More importantly, the variations of spectral response among simulated samples (measured by the separation of confidence bands) along period are very much comparable with what can be expected had the samples been generated using strictly Priestley process based simulation (see [12]). Hence the inter-sample variability is not actually compromised at the response level by imposing localization of narrowband-limited white-noise and level-wise total energy matching. The recorded motion and two simulated random samples are shown in Fig.3. It is clear from the figure that the temporal features of random samples have adequate variability such that neither they look identical nor they look completely different from the recorded signal.

3. Scenario-based Energy Arrival Scaling Model

Ground motions specific to a seismic scenario can be generated by knowing energy arrival patterns $\bar{E}_j(b)$ for that scenario. A scaling model for $\bar{E}_j(b)$ based on seismological parameters is developed using energy arrival patterns $\bar{E}_j(b)$ extracted from the recorded ground motions. Hence, a scenario-specific energy arrival can be estimated along with its aliatory uncertainty. The uncertainty will arise because which particular recording process a scenario might represent is inherently random. Scenario specific ensembles of motions will, therefore, exhibit varied frequency dependent amplitude modulations resulting from different recording processes. The scaling relationship for $\bar{E}_j(b)$ is considered as

$$\ln(\bar{E}_j(b)) = a_{1,j}(b)M + a_{2,j}(b)\ln\Delta + a_{3,j}(b)S + a_{4,j}(b) ; \forall j \quad (12)$$

where, M is the local magnitude, Δ is the representative source-to-site distance due to Trifunac and Lee [17, 18], S is the indicator parameter for local site conditions ($S=0, 1$ and 2 for soft soil, stiff soil and rock, respectively). The representative distance Δ takes the finite source dimension into account and in general depends on M , epicentral distance (R), focal depth (h), time period of seismic wave and shear wave velocity of local site (180 m/s, 270 m/s, 850 m/s for $S=0, 1$ and 2 , respectively).

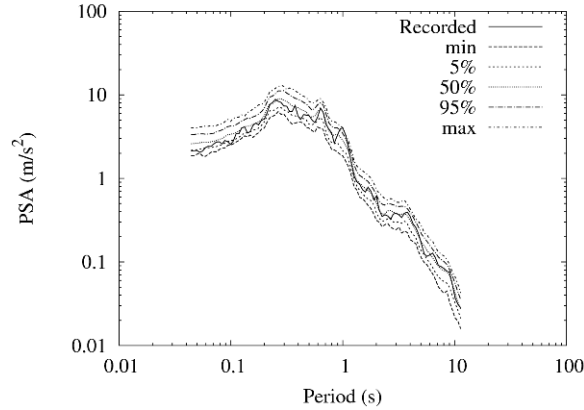


Fig. 2 - Recorded PSA Spectrum along with PSA Spectra for different Levels of Confidence from Simulation

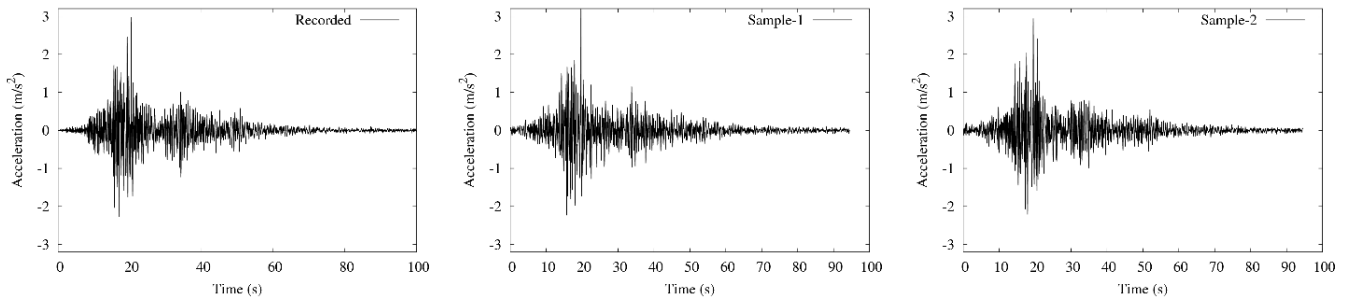


Fig. 3 - Comparison of the Chi-Chi Motion Recorded at Station C041 along East-West Direction and Two Random Samples

The database for the regression analysis comprises north-south component of main shock (93 number of recordings) and aftershocks of magnitude 5 and above (394 number of recordings) during the 1999 Chi-Chi earthquake [19, 20]. These aftershock records are chosen such that all recordings are within 50 km of the corresponding epicentral distance (with acceptable signal to noise ratio). The main shock recording at a station is considered only if at least one aftershock recording is chosen for the station, otherwise, the majority of epicentral distances of main shock from the respective recording stations would be higher than 50 km and the distant motion prediction may get biased towards the main shock. The maximum value of b is taken as 100 s for all the records to maintain uniformity irrespective of their recorded length. The minimum value of b is considered to be -12 s. It is understood that smaller records will converge to its 100% energy arrival for a smaller value of b than a lengthy record. Further, for estimation of regression coefficients b is discretized every 0.02 s of interval. Maximum likelihood method [21] is used to carry out the regression analysis and the error, $\varepsilon_j(b)$, in the scaling model is defined as

$$\varepsilon_j(b) = \ln(\bar{E}_j(b)) - \ln(\hat{E}_j(b)) ; \forall j \quad (13)$$

where, $\hat{E}_j(b)$ is the estimated (smooth) energy arrival using Eq. (12) via estimated smoothed regression coefficients. Further, $\varepsilon_j(b)$ is a normal variate with mean zero and standard deviation $\sigma_j(b)$.

The coefficient $a_{1,j}(b)$ is positive for all values of j and b , similarly $a_{2,j}(b)$ and $a_{3,j}(b)$ are found to be negative throughout. This shows the soundness of the coefficients because energy arrival should increase with increasing earthquake magnitude and decrease with increasing source-to-site distance and also the energy arrival should increase in presence of soft soil due to local site amplification. All regression coefficients for $j = -12$ and $j = -4$ are shown in Fig.4 as example. The variation of the regression coefficients along b affects the change of shape of the energy arrival pattern which in-turn affects the level-wise SMD, defined as the duration corresponding to the central 90% level-wise energy arrival [3]. These SMDs obtained from $\hat{E}_j(b)$ have been found to increase with increasing magnitude and distance, and decrease if local site changes from soft soil to rock type; a fact that further validates the soundness of the coefficients.

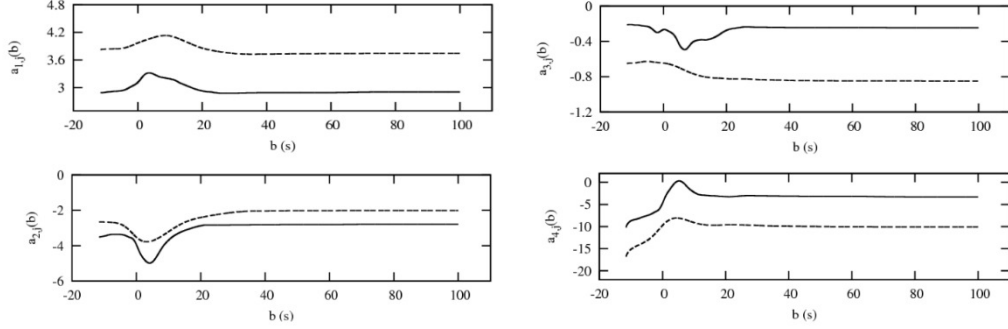


Fig. 4 - Regression Coefficients for $\ln(\bar{E}_j(b))$ in the Cases of Levels $j = -12$ (solid line) and $j = -4$ (dotted line)

4. Generation of Scenario specific ensemble of ground motions

For a given scenario, the predicted energy arrival pattern for any level j will have some inherent uncertainty as discussed before. The prediction error depends only on one parameter $\sigma_j(b)$, the level-wise standard deviation of $\varepsilon_j(b)$. Hence, the i th sample for the level-wise energy arrival for a given seismic scenario can be modelled as

$$\ln(\hat{E}_{i,j}(b)) = \ln(\hat{E}_j(b)) + k_i \sigma_j(b) ; \forall j \quad (14)$$

where, k_i is the sample specific realization of a standard normal variate. k_i is made level independent so that the time-frequency characteristics of a simulated motion from $\hat{E}_{i,j}(b)$ s remain realistic, otherwise only one or a few narrowband waves can dominate the simulated motion – a phenomenon that has never been observed in the recorded data set. Further, the standard deviation of $\varepsilon_j(b)$ is smoothed along b before applying in Eq. (14) so that the extracted $V_j(b)$ remains slow varying. Even though $\hat{E}_{i,j}(b)$ should be a non-decreasing function of b , some local anomaly may arise occasionally where the energy arrival curve is expected to be quite flat. To rectify this local anomaly, $\hat{E}_{i,j}(b)$ is forcefully made non-decreasing by replacing any local depression with horizontal trend. From the $\hat{E}_{i,j}(b)$ s, ground motions are simulated by the same method discussed in Section 2.2.

It is interesting to see if the samples generated by the above method can represent the expected trend. For this purpose the median trend of response spectra, obtained from different scenario specific ensembles, have been compared with those obtained directly from a GMPE developed using the same database. The regression coefficients of a PSV scaling model is obtained using the maximum likelihood method [21], and the mathematical form of the scaling model is chosen as

$$\ln(PSV(T)) = b_1(T)M + b_2(T) \ln \Delta + b_3(T)S + b_4(T) \quad (15)$$

through the same independent parameters as considered for modelling $\bar{E}_j(b)$. The error in estimation of the scaling model is defined as

$$\varepsilon_{PSV}(T) = \ln(PSV(T)) - \ln(\widehat{PSV}(T)) \quad (16)$$

where, $\ln(\widehat{PSV}(T))$ is the estimated PSV using Eq. (15) through estimated smooth regression coefficients. Further, $\varepsilon_{PSV}(T)$ is normal variate with mean zero and standard deviation $\sigma_{PSV}(T)$.

For the numerical comparison, 500 ground motion samples are generated for two hypothetical seismic scenarios – Scenario 1 ($M = 5.5, R = 30 \text{ km}, h = 10 \text{ km}, S = 1$) and Scenario 2 ($M = 7.3, R = 50 \text{ km}, h = 10 \text{ km}, S = 0$). The values for Δ are computed accordingly [17, 18] for the two scenarios. Fig.5(a) shows the median estimates of PSV spectra from samples and the median estimates from PSV scaling model for the two scenarios. It can be seen from the figure that the median estimates of the PSV spectra from simulated ensemble are in reasonable agreement with the median estimates from the PSV scaling model.

The standard deviation of $\ln PSV(T)$ for the simulated ensemble is obtained so that it can be compared with $\sigma_{PSV}(T)$ of PSV scaling model and are shown in Fig.5(b). The uncertainties of PSV spectra separately obtained from a PSV scaling model and from a scenario-specific ensemble are not compatible with each other. The PSV model is regressed using one data per seismic scenario, and hence, the inherent uncertainty is computed considering all scenarios. For the same reason the aliatory uncertainty of a GMPE is essentially scenario independent. For the scenario specific ensemble, there are two types of uncertainty; (i) recording process represented by the scenario is uncertain, (ii) level-wise sample of a given recording process is uncertain. Also due to positive or negative interference of different decomposed waves in the composite ground motion, there is additional variability. These all make the variability of PSV spectra among an ensemble not only scenario dependent but also higher than that directly obtained from the PSV model. It is clear that the trends of standard deviations along period are quite similar in all the cases, though their values corresponding to the ensembles are different for different scenarios.

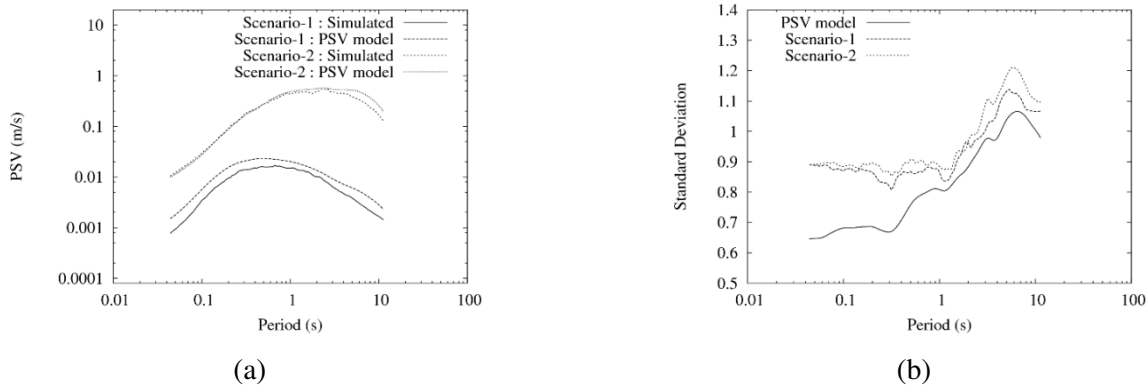


Fig. 5 - Comparison of (a) Median Spectra and (b) Standard Deviations of PSV spectra obtained from the Simulated Ensembles and from the PSV Scaling Model for Two different Scenarios

Two random samples each for Scenario 1 and Scenario 2 are shown in Fig.6. The samples for each scenario show variabilities in the temporal features and the strength, as expected. The median SMD of 500 samples for Scenario 1 is 21.95 s and that for Scenario 2 is 40.09 s. This shows that the median SMD of an ensemble is following the expected trend with respect to seismic scenario, because SMD for a smaller and nearer event (like Scenario 1) is likely to be smaller than that for a larger and farther event (like Scenario 2).

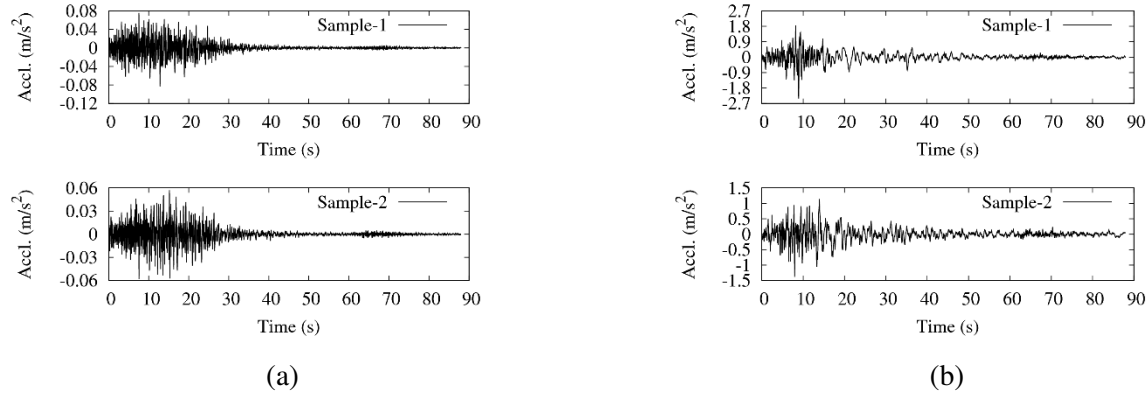


Fig. 6 - Two Arbitrarily Selected Random Samples for (a) Scenario 1 and (b) Scenario 2

5. Generation of GMPE-compatible ensemble of ground motions

The simulated ensemble of ground motions have varied time-frequency characteristics which can provide a platform for scenario specific nonlinear response statistics, provided median estimate of spectral response along with its variability match with those of a target GMPE. A new algorithm is hence developed wherein the estimated energy arrival $\hat{E}_j(b)$ and the model uncertainty $\sigma_j(b) \forall j$ are modified such that a scenario specific ensemble becomes compatible to any target GMPE, both in terms of median estimate and standard deviation. To facilitate the generation of GMPE-compatible ground motions, Eq. (14) is modified as follows:

$$\ln(\hat{E}_{i,j}(b)) = \ln(\hat{E}_j(b)) + \ln(\alpha_{1,j}) + \alpha_{2,j}k_i\sigma_j(b) ; \forall j \quad (17)$$

Here, $\alpha_{1,j}$ is a level-wise factor used to scale up/down the total energy such that the median PSV of the simulated motions matches with that of the target PSV model and, $\alpha_{2,j}$ is another level-wise factor used to scale up/down $\sigma_j(b)$ such that standard deviation of the PSV from the simulated motions matches (with some tolerance) that of the target one.

To demonstrate this GMPE-compatibility method, 200 motions are simulated using Eq. (17) and the same PSV scaling model as in Eq. (15) is used as the target, arbitrarily. The tuning algorithm will work for any target PSV model other than the one developed using the same database. However, the simulated compatible ensemble will have the scenario dependent temporal features corresponding to the database used for the development of energy arrival scaling model and not corresponding to the database using which target GMPE is developed. Fig.7(a) and 7(b) show the results for the same quantities as shown in Fig.5(a) and 5(b), respectively, with only exception that the GMPE-compatible case is added to them. Further, Fig.8 shows the PSV values corresponding to different confidence levels from the ensembles for Scenario 2 along with the theoretical estimates from the PSV scaling model (from $\overline{PSV}(T)$ and $\sigma_{PSV}(T)$). It can be seen that, proposed simulation technique naturally matches the distribution of PSV from GMPE-compatible ensemble with that of the target PSV model when only median and standard deviation are targeted. This is because both the regression models for PSV and energy arrival curves follow Gaussian distribution for aliatory uncertainties. Such an acceptable match of distribution is also achieved, from the same ensemble, when PSV models are developed for damping ratios ranging from 2% to 10%. It may be noted here that PSV and PSA differ only by a constant factor for a specific time period and hence, the period specific statistics of them are having one to one correspondence and in logarithmic scale their standard deviations are identical. Thus, the proposed simulation technique is equally applicable with PSA scaling model with identical quality of match.

It will be interesting to study the statistics of nonlinear response using the scenario-specific ensemble (without GMPE compatibility) and GMPE-compatible ensemble for the same scenario. For nonlinear analyses, an elasto-perfectly-plastic (EPP) oscillator with yield force F_y , and yield displacement X_y are used. For damage characterization, ductility demand and normalized hysteresis energy (normalized by $F_y X_y$) are believed to be two

important parameters. For that reason the constant ductility PSA spectrum with (ductility demand) $\mu = 4$ and the corresponding normalized hysteresis energy spectrum are considered as the two nonlinear response quantities for the purpose of comparison. Fig.9(a) and 9(b), respectively, show the nonlinear PSA spectra and the normalized hysteresis energy spectra corresponding to different confidence levels for the scenario-specific and GMPE-compatible simulated ensembles in the case of Scenario 2. As expected, the distribution of any nonlinear response in the case of scenario-specific ensemble is different from that in the case of GMPE-compatible, though their variation along initial period of EPP oscillators is very similar. Moreover, the difference of distribution in the case of normalized hysteresis energy is not very significant. Further, for higher confidence level the constant ductility spectra from the two different ensembles are coming close to each other especially for initial periods beyond 0.3 s. This suggests that the proposed methodology to obtain scenario-specific ensemble, without tuning to any GMPE (developed for the same region), can produce hazard-consistent statistical estimate for damage estimation associated with higher level of confidence.

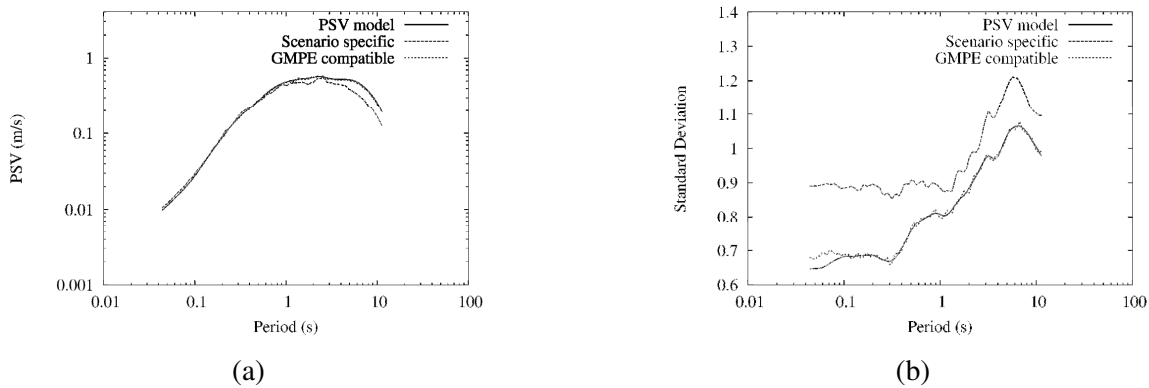


Fig. 7 - Comparison of Median PSV Spectra and Standard Deviations obtained from Scenario-Specific and GMPE-Compatible Ensembles for Scenario 2

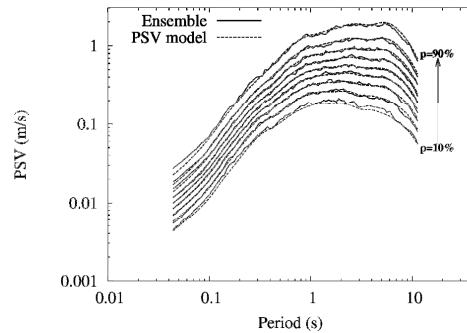


Fig. 8 - Comparison of different Percentile PSV Spectra obtained from GMPE-Compatible Ensemble and PSV scaling model for Scenario 2

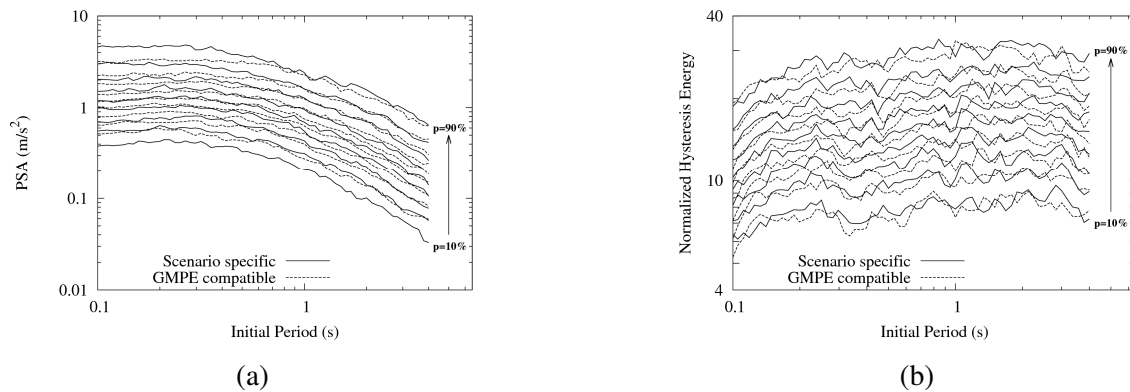


Fig. 9 - Comparison of (a) different Percentile Nonlinear PSA Spectra and (b) different Percentile Normalized Hysteresis Energy Spectra obtained from Scenario-Specific and GMPE-Compatible Ensembles for Scenario 2

6. Conclusions

A new method for simulation of process-specific ground motions has been developed using level-wise instantaneous energy arrival of wavelet coefficients. It has been found that simulated motions for a specific recording process capture the temporal characteristics of the recorded motion and also give desirable sample to sample variability at the linear response level. Then a scaling model has been developed for the energy arrival curve in terms of seismological parameters to produce scenario-specific ensemble of accelerograms. The median estimates of PSV of the ensemble are found to be comparable with those directly obtained from the PSV scaling model. Finally, a new algorithm has been proposed to modify the estimated energy arrival curves so that the simulated ensemble produces medians and standard deviations of PSV same as those of the target. The GMPE-compatible ensemble is found to be in good agreement with PSV scaling models developed for a wide range of damping ratio. The proposed methodology is equally applicable when a PSA scaling model is used instead of PSV. The scenario-specific ensemble, without explicit GMPE-compatibility, produces comparable nonlinear response statistics with respect to GMPE-compatible ensemble corresponding to lower probability of exceedance. Hence, in such cases the explicit GMPE-compatibility may be avoided. Nevertheless, the current study will provide GMPE-compatible ground motions for direct statistical estimation of any nonlinear response.

The attenuation models proposed or used in the present study are kept simple but viable in order to demonstrate various aspects of the proposed methodologies of ground motion simulation. Further, the conclusion on avoidance of GMPE-compatibility may differ if the PSV scaling model is developed using different functional form or data than what is used for developing the scaling model of energy arrival.

7. Acknowledgement

The authors would like to acknowledge the financial support provided by the Department of Science and Technology, India, under the sanction number DST/TSG/STS/2012/55-G.

8. References

- [1] Campbell KW, Bozorgonia Y (2008): NGA ground motion model for the geometric mean horizontal component of PGA, PGV, PGD and 5% damped linear elastic response spectra for periods ranging from 0.01 to 10s. *Earthquake Spectra*, **24** (1), 139-171.
- [2] Atkinson GM, Worden CB, Wald DJ (2014): Intensity prediction equations for North America. *Bulletin of the Seismological Society of America*, **104** (6), 3084–3093.
- [3] Trifunac M, Brady A (1975): A study on the duration of strong earthquake ground motion. *Bulletin of the Seismological Society of America*, **65** (3), 581–626.
- [4] Golafshani A, Bakhshi A, Tabeshpour M (2005): Vulnerability and damage analysis of existing

- buildings. *Asian Journal of Civil Engineering (Building and Housing)*, **6** (1-2), 85–100.
- [5] Mollaioli F, Bruno S, Decanini L, Saragoni R (2011): Correlations between energy and displacement demands for performance-based seismic engineering. *Pure and Applied Geophysics*, **168** (1-2), 237–259.
- [6] Yamamoto Y, Baker JW (2013): Stochastic model for earthquake ground motion using wavelet packets. *Bulletin of the Seismological Society of America*, **103** (6), 3044–3056.
- [7] Vetter C, Taflanidis A, Mavroeidis GP (2015): Tuning of stochastic ground motion models for compatibility with ground motion prediction equations. *Earthquake Engineering and Structural Dynamics*, **45**, 893-912.
- [8] Wang G (2011): A ground motion selection and modification method capturing response spectrum characteristics and variability of scenario earthquakes. *Soil Dynamics and Earthquake Engineering*, **31** (4), 611–625.
- [9] Tarbali K, Bradley B (2015): Ground motion selection for scenario ruptures using the generalized conditional intensity measure (GCIM) method. *Earthquake Engineering and Structural Dynamics*, **44** 1601–1621.
- [10] Kwong N, Chopra AK, McGuire R (2015): A framework for the evaluation of ground motion selection and modification procedures. *Earthquake Engineering and Structural Dynamics*, **44** 795–815.
- [11] Priestley MB (1965): Evolutionary spectra and non-stationary processes. *Journal of the Royal Statistical Society. Series B (Methodological)*, 204–237.
- [12] Conte J, Peng B (1997): Fully nonstationary analytical earthquake ground-motion model. *Journal of Engineering Mechanics*, **123** (1) 15–24.
- [13] Das S, Gupta VK (2011): A wavelet-based parametric characterization of temporal features of earthquake accelerograms. *Engineering Structures*, **33** (7) 2173–2185.
- [14] Iyama J, Kuwamura H (1999): Application of wavelets to analysis and simulation of earthquake motions. *Earthquake Engineering and Structural Dynamics*, **28** 255–272.
- [15] Basu B, Gupta VK (1998): Seismic response of sdof systems by wavelet modelling of nonstationary processes. *Journal of Engineering Mechanics*, **124** (10) 1142–1150.
- [16] Spanos PD, Failla G (2004): Evolutionary spectra estimation using wavelets. *Journal of Engineering Mechanics*, **130** (8) 952-960.
- [17] Trifunac M, Lee V (1990): Frequency dependent attenuation of strong earthquake ground motion. *Soil Dynamics and Earthquake Engineering*, **9** (1) 3–15.
- [18] Trifunac M, Lee V (1989): Empirical models for scaling pseudo relative velocity spectra of strong earthquake accelerations in terms of magnitude, distance, site intensity and recording site conditions. *Soil Dynamics and Earthquake Engineering*, **8** (3) 126–144.
- [19] Lee W, Shin T, Wu C (2001): CWB free-field strong-motion data from 30 early aftershocks of the 1999 Chi-Chi earthquake: Processed acceleration data files on CD-ROM, CWB strong-motion data series CD-003, Seismological Observation Center of Central Weather Bureau: Taipei, Taiwan.
- [20] Lee W, Shin T, Wu C (2001): CWB free-field strong-motion data from three major aftershocks of the 1999 Chi-Chi earthquake: Processed acceleration data files on CD-ROM, CWB strong-motion data series CD-002, Seismological Observation Center of Central Weather Bureau: Taipei, Taiwan.
- [21] Joyner WB, Boore DM (1993): Methods for regression analysis of strongmotion data. *Bulletin of the Seismological Society of America*, **83** (2) 469–487.